Reactive and Nonreactive Quenching of OH(A $^2\Sigma^+$) in Collisions with H Atoms†

George C. Schatz,* Brent Fisher, Will Grande, Ken Kumayama, and Lisa A. Pederson

Department of Chemistry, Northwestern University, Evanston Illinois 60208-3113

Received: August 29, 2000; In Final Form: November 15, 2000

We use trajectory surface hopping methods to calculate cross sections and rate coefficients for reactive and nonreactive quenching of OH(A $^2\Sigma^+$) in collisions with H atoms. All calculations are based on multireference configuration interaction potential surfaces for the $1^1A'$ and $2^1A'$ surfaces of water, using a diabatic representation to describe electronic transitions. The overall rate of quenching plus reaction is in good agreement (lower by 25−30%) with earlier estimates at 300 and 1500 K. Analysis of the trajectories shows that this rate is dominated by a capture mechanism on the $2^1A'$ state of water, with a nearly unity probability for hopping to the $1^1A'$ state following formation of a short-lived collision complex. Both reactive and nonreactive decay of the complex are significant, with branching to H + OH (nonreactive quenching), H + OH (atom exchange with quenching), and O(^{1}D) + H_2 (reaction) accounting for approximately 45%, 35%, and 20%, respectively, of the product yield. The cross section for atom exchange without quenching is only 1−3% of the total quenching/reaction cross section. In contrast to what is often assumed in energy transfer studies, we find that the quenching and reactive cross sections are very weakly dependent on OH rotational quantum number for quantum numbers in the range 0−15. A statistical model provides only a rough description of product branching and product energy partitioning, indicating that the intermediate complexes are too short-lived to show statistical dynamics. We find that pure rotational energy transfer cross sections are small (few percent) compared with quenching/reaction.

I. Introduction

Laser induced fluorescence measurement of hydroxyl radical concentrations is now a standard tool for combustion diagnostics.[1] In this measurement, any nonradiative process that removes (quenches) the OH(A $^2\Sigma^+$) (hereafter referred to as OH(A)) intermediate state must be accounted for if quantitative estimates of hydroxyl concentrations are to be made. In addition, the rates of rotational energy transfer within the A state manifold must also be known. Under typical flame conditions, quenching and energy transfer arise from collisions of OH(A) with a variety of species. Most of these are stable molecules (N_2, O_2, H_2O, CO_2) for which the relevant rate coefficients either are known from kinetics measurements [2] or may be estimated from simple models.[3] Transient radical species may also contribute, but most of the quenching and energy transfer rates for such species are not known, due to the difficulty in performing measurements on radical plus OH(A) collisions.

Of the possible transient species in combustion processes, H atoms are thought to play a significant role in quenching of OH(A), accounting for >50% of OH(A) removal in some flames.[4] However, the relevant rate coefficients are poorly known, having only been measured at room temperature[5] or inferred indirectly from combustion modeling.[6] In addition, nothing is known about the branching between nonreactive quenching and quenching with hydrogen atom exchange in H + OH(A) collisions, about whether O(^{1}D) + H_2 is an important product, about the dependence of the quenching rate coefficients on OH(A) rotational state, and about the significance of pure rotational energy transfer.

Recently it has become possible to use theoretical methods to determine the rates of quenching and energy transfer in the H + OH(A) system. This has come about for two reasons. First, global potential energy surfaces and their couplings have now been determined using high-quality multireference configuration-interaction methods for the first three singlet states of water (1A′, 1A″, and 2A′).[7] Figure 1, which shows a schematic of the 1A′ and 2A′states for linear HHO and HOH geometries, indicates that 2A′ correlates to H + OH(A), while 1A′ provides the final state for quenching, atom exchange, and reaction to give O(^{1}D) + H_2. O(^{1}D) + H_2 can also be formed adiabatically on the 2A′ state. Second, dynamics methods have become available for studying reaction and other processes for the lowest states of water using either wave packets or trajectory surface hopping (TSH).[8,9] These potential surfaces and dynamics methods have already been used in studies of nonadiabatic dynamics in the O(^{1}D) + H_2 reaction,[8−10] where it has been found that coupling between the 2A′ and 1A′ states is significant, and this leads to measurable contributions to the reactive cross sections, angular distributions, and final state distributions.

In this paper we present the results of a theoretical study of quenching and energy transfer in the H + OH(A) system. This study has used accurate potential surfaces for the 1A′ and 2A′ states of water, along with TSH methods, to determine cross sections, rate coefficients, and other dynamical information of relevance to LIF measurements of OH concentrations. The 1A″ state, which correlates to H + OH(X) and to O(^{1}D) + H_2 (see Figure 1) and which couples to 1A′ and 2A′ only by Coriolis-induced transitions, is not included. Although 1A″ could be populated toward the end of the collisions that undergo quenching, it is unlikely to influence the overall quenching rate or the branching between the various product channels. We also omit the triplet state that correlates to H + OH(A), as this is likely to be more repulsive than 2A′ and thus should be less important to the measured quenching rates.

† Part of the special issue "William H. Miller Festschrift".

10.1021/jp003092n CCC: $20.00
Published on Web 01/10/2001

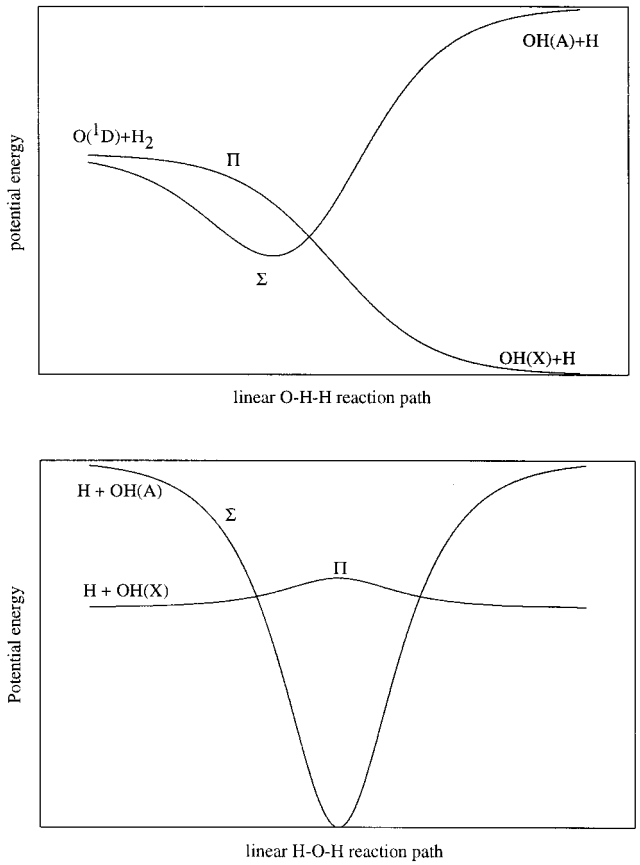

Figure 1. Schematic of potential energy along reaction path for the 1A′ and 2A′ states of water. Top panel shows linear HHO geometries, and bottom shows linear HOH geometries. The 1A′ (2A′) potential is the lesser (greater) of the Σ and Π potentials for each geometry.

The next section describes the potential surfaces and couplings and the dynamics methods that we have used. Section III presents the cross sections and rate coefficients, and section IV summarizes our conclusions.

II. Potential Surfaces and Dynamics

A. Potential Surfaces. The 1A′ and 2A′ surfaces and couplings are from the large-scale multireference configuration interaction calculations of Dobbyn and Knowles (DK).[6] Although the properties of these surfaces have been described previously,[6−9] the applications to H + OH(A) involve several aspects that are new, so we give additional details here.

The DK surfaces have been developed in a diabatic representation, which means that we are provided with a 2 × 2 matrix of surfaces whose eigenvalues are the 1A′ and 2A′ surfaces. The coupling term V_{12} in this matrix vanishes for H−O−H and H−H−O linear geometries, which means that one of the diagonal elements of this matrix becomes the Σ potential for these geometries and the other becomes the Π potential. We will use these labels for all geometries, referring to the two diabats as Σ-like (V_Σ) and Π-like (V_Π). Since the TSH dynamical calculations will use the diabatic representation for all calculations, it is important to examine V_Σ, V_Π, their coupling surface, and their intersection seam, to understand what happens during collisions.

Figure 2 presents a contour plot of V_Σ and V_Π, using a coordinate system in which the OH is located on the *y* axis, with its center of mass at the origin and the H is in the positive *y* direction. The contours refer to the location of the second H atom relative to this coordinate system. The OH distance *r* has been fixed at 1.9 a_0, which is close to its equilibrium distance. This choice makes Figure 2 appropriate for describing the initial approach of the reacting species. Figure 2a is the Σ-diabat, which means that it correlates to the A state potential in the limit of infinite separation between H and OH. This H + OH(A) energy is 44 kcal/mol in the figure, which is the energy relative to O(^{1}D) + H_2 (which is taken to be zero energy). The Σ-diabat also

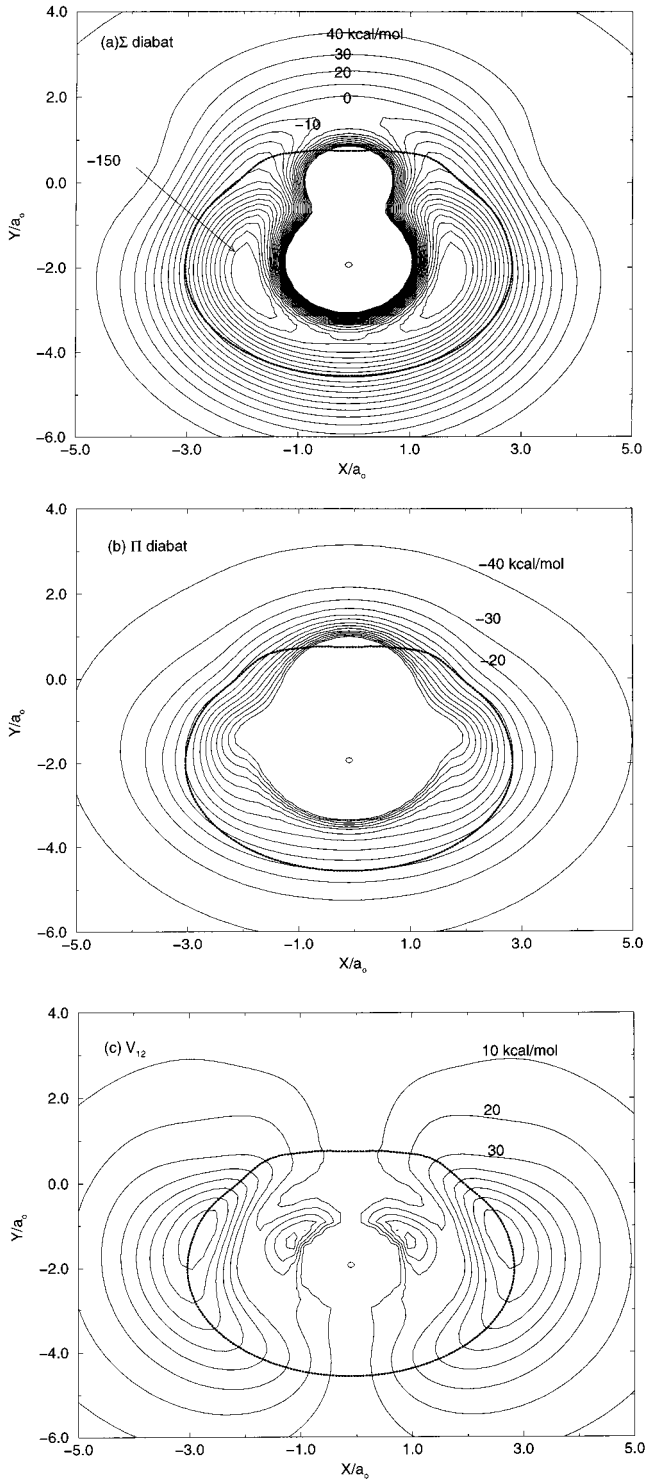

Figure 2. Contours of the DK potential surfaces for H_a + OH_b as a function of the H_a Cartesian coordinates, with the OH_b fixed along the *y* axis with the OH_b distance taken to be 1.9 a_0. Included are (a) the Σ-diabat, (b) the Π-diabat, and (c) the coupling surface V_{12}. In (a) and (b), the seam of intersection between the two diabats in shown with a thick dotted curve. In all plots, the contour interval is 10 kcal/mol, with the energy for selected contours indicated.

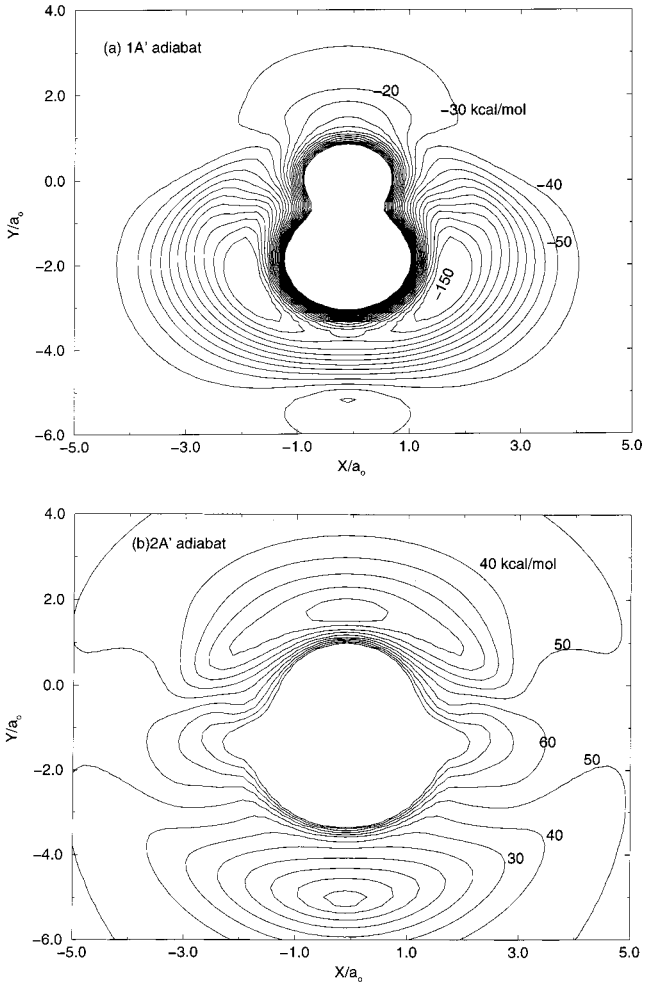

Figure 3. Contours of the DK potential surfaces, using the same format as in Figure 2, but showing the adiabats (a) 1A′ and (b) 2A′.

correlates to the deep water molecule well (with an energy of about −150 kcal/mol for the chosen value of the OH distance). Figure 2a shows that the Σ-diabat is attractive for all orientations. The corresponding Π-diabat, shown in Figure 2b, is completely repulsive around the OH. This potential correlates to the ground state of OH, so its asymptote is at −42 kcal/mol, corresponding to 86 kcal/mol below the OH(A) + H asymptote of V_Σ. The crossing seam between the diabats is shown in Figure 2a,b, and we see that it occurs on the outer wall of the well in the Σ-diabat at an energy of about −60 kcal/mol relative to O(^{1}D) + H_2. The seam will therefore be encountered in the initial addition process, but even if hopping does not occur then, the seam will be crossed each time the water molecule vibrates. Figure 2c shows that the coupling surface V_{12} is large near the crossing seam for all but linear geometries.

Figure 3 shows the adiabats V(1A′) and V(2A′) for the same geometry as in Figure 2. These contours show that the 2A′ adiabat is attractive for all but perpendicular approach of H to OH, while the corresponding 1A′ adiabat is attractive for all but linear approach to either end of OH. The HHO and HOH wells of the 2A′ adiabat form the upper cone of the conical intersection between the two adiabats, while the bottom of each cone shows up as a repulsive maximum in the 1A′ surface.

B. Dynamics Calculations. The TSH calculations have used the "fewest switches" method of Tully,[11] with a few minor revisions as described by Schatz and co-workers.[8,12,13] One important change that was previously described in ref 8 is the use of a diabatic representation rather than an adiabatic representation for the electronic states. This means that we use V_Σ and V_Π to integrate trajectories and V_{12} to determine the coupling that goes into the time-dependent Schrödinger equation. In previous work[8] we found that this provides more accurate results than the adiabatic representation if the dynamical process is closer to being diabatic than adiabatic. By "closer" we mean that there are fewer hops in the diabatic representation. In the present application, both adiabats and diabats give rise to attractive long-range potentials in the initial approach of H to OH, so the overall cross section should be similar. We find that, in most trajectories that access the attractive wells, the number of hops in the diabatic representation is usually in the range 1−5, and most of these hops are well separated in time. These are conditions that are favorable for the diabatic representation.

The TSH calculations have been performed with a maximum impact parameter of 9.5 a_0. Larger values were tested, but we find that this value converges both quenching and rotational inelastic cross sections. Usually 5000 trajectories have been integrated for each translational energy and initial OH rotational quantum number. The electronic angular momentum has been neglected in defining this OH rotational quantum number. Only vibrational ground state collisions have been considered. Boltzmann averaging of cross sections has been performed by fitting the cross section to a simple function of the translational energy E_T (usually $A + B/E_T^c$, where A, B, and c are constants), and then doing the integral analytically.

We have also performed capture theory calculations of the total quenching cross section. Reference 8 describes the general theory. In the present calculation, the maximum impact parameter for which the centrifugal barrier energy (the maximum in the sum of potential energy plus centrifugal energy) matches the translational energy is determined numerically, and then the cross section is equated to πb_{max}^2. The potential energy in this calculation is equated to the Σ-diabat, evaluated for OH at equilibrium, and assuming a linear HOH orientation. This choice of orientation yields the most attractive potential, which means that the cross sections we obtain should be upper bounds to the correct values. This choice of orientation is what would be appropriate if the OH is able to reorient to the lowest energy structure while the H atom approaches. We also studied other choices, such as averaging over fixed angle cross sections (equivalent to a rotational sudden approximation), but found that the linear HOH orientation assumption yielded results in best overall agreement with the trajectory results, so this is what will be presented. We have also tested the capture model using the 2A′ adiabat rather than the Σ-diabat. Of course, for the linear HOH orientation assumption there is no difference between 2A′ and Σ-diabat. Other choices for orientation averaging on 2A′ did not yield better overall results.

III. Results

A. Cross Sections for Quenching and Reaction. Let us define the cross sections that we will present and discuss as follows:

1. σ_T = total cross section for quenching and reaction
2. σ_{NQ} = cross section for nonreactive quenching
3. σ_{XQ} = cross section for quenching with hydrogen atom exchange
4. σ_R = total cross section for reaction to give O(^{1}D) + H_2
5. σ_{R1} = contribution to σ_R from trajectories that end up on the 1A′ final electronic state of O(^{1}D) + H_2
6. σ_{R2} = contribution to σ_R from trajectories that end up on the 2A′ final electronic state of O(^{1}D) + H_2

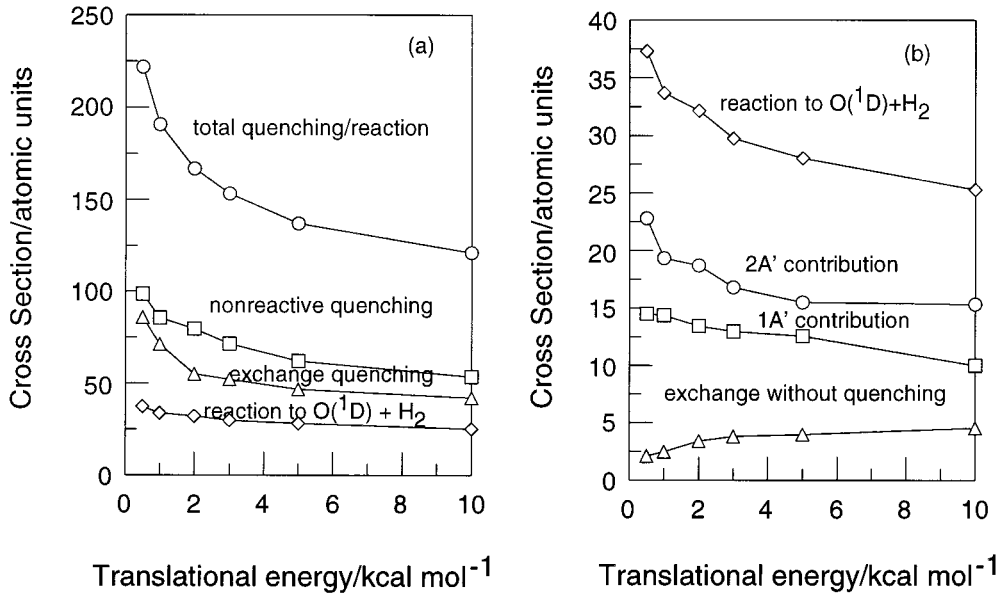

Figure 4. TSH cross sections for $N = 0$ as a function of translational energy for H + OH(A). The curves in (a) are total quenching plus reaction (circles), nonreactive quenching (squares), quenching with H atom exchange (triangles), and total reaction to $O(^1D) + H_2$ (diamonds), while in (b) the curves are total reaction to $O(^1D) + H_2$ (diamonds), $O(^1D) + H_2$ (2A′ contribution) (circles), $O(^1D) + H_2$ (1A′ contribution) (squares) and atom exchange without quenching (triangles).

TABLE 1: TSH Cross Sections for H + OH(A) at 2 kcal/mol Translational Energy, along with Product Energy Partitioning Information from TSH and from the Microcanonical Model

	TSH results					microcanonical results			
event	cross section (a_0^2)	branching fraction	E_{trans} (kcal/mol)	E_{vib} (kcal/mol)	E_{rot} (kcal/mol)	branching fraction	E_{trans} (kcal/mol)	E_{vib} (kcal/mol)	E_{rot} (kcal/mo l)
NQ	79.6	0.47	42.9	42.0	14.8	0.47	39.5	24.1	30.5
XQ	55.1	0.32	41.3	44.7	13.7	0.47	39.5	24.1	30.5
R	32.1	0.19	23.5	13.9	16.5	0.06	21.1	10.6	18.2
R1	13.4	0.08	21.8	13.7	18.5	0.03	21.1	10.6	18.2
R2	18.7	0.11	24.7	14.1	14.9	0.03	21.1	10.6	18.2
X	3.4	0.02	0.6	0	1.5	9.8×10^{-5}	0.6	0	0.4

7. σ_X = cross section for atom exchange without quenching

8. σ_{NR}= nonreactive rotationally inelastic cross section without quenching

Note that $\sigma_T = \sigma_{NQ} + \sigma_{XQ} + \sigma_R$ and also $\sigma_R = \sigma_{R1} + \sigma_{R2}$. Obviously atom exchange is not a distinguishable process for OH(A) + H, but we have calculated the cross sections as if it were to provide physical insight. This is also true for the two cross sections that lead to formation of $O(^1D) + H_2$. σ_X and σ_{NR} do not contribute to the removal of OH(A), so we have not included these in calculating σ_T. For each of the processes listed above, we have calculated cross sections as a function of E_T, and as a function of the OH rotational quantum number J. Here we use J rather than the usual "N" to avoid confusion with the "N" that is used to denote "nonreactive". Similarly, the final OH rotational state will be denoted J'.

Figure 4 presents TSH cross sections for $J = 0$ for the first seven processes mentioned above as a function of E_T. These cross sections have not been multiplied by an electronic degeneracy factor, but later we present σ_T with the 1/4 weighting associated with the singlet initial state factored in. Error bars are not given, but typically they are ±1%, ±3%, ±3%, ±4%, ±6%, ±6%, and ±16% for the seven processes.

Figure 4a shows that σ_T is a decreasing function of E_T, with a very large value (around 200 a_0^2 at 1 kcal/mol). We also see that all of the processes 2−4 listed above contribute significantly to σ_T, and all of these have about the same dependence on E_T. The largest contribution is from nonreactive quenching, which accounts for about 45% of the total. Second largest is from quenching with atom exchange, accounting for 35%, and then reaction accounts for 20%. Figure 4b shows that both surfaces contribute about equally to the reactive cross section. The cross section σ_X (exchange without quenching) is less than 4% of σ_T over the range of energies considered. Although this process is the only one of processes 1−7 that can take place without any hops, we see that it is a very minor process in the dynamics. This result would arise if essentially every collision that contributes to any of the seven processes listed above, i.e., trajectories which cross the centrifugal barrier, involved formation of an intermediate complex. This is the expected behavior given the appearance of the Σ-diabat in Figure 2a. In addition, if complex formation is linked to quenching/reaction, then it follows that the cross sections in Figure 4 should all have the same dependence on E_T, and also that the probabilities of the events 2−6 might be modeled by a statistical model.

To test if a statistical model is appropriate for the branching in Figure 4, we have calculated microcanonical statistical probabilities for each of the events 2−7 using standard expressions.[14] The resulting branching at 2 kcal/mol is listed in Table 1, along with other results that will be described later. We see that statistical theory predicts $\sigma_{NQ} = \sigma_{XQ}$ and $\sigma_{R1} = \sigma_{R2}$, which is approximately what the calculated results show. In addition, the branching between exchange and reaction to $O(^1D) + H_2$ is in the right direction, though predicting more exchange and less reaction than we actually find. We conclude that statistical theory provides at least a zero-order description of the branching in this problem. The higher than statistical

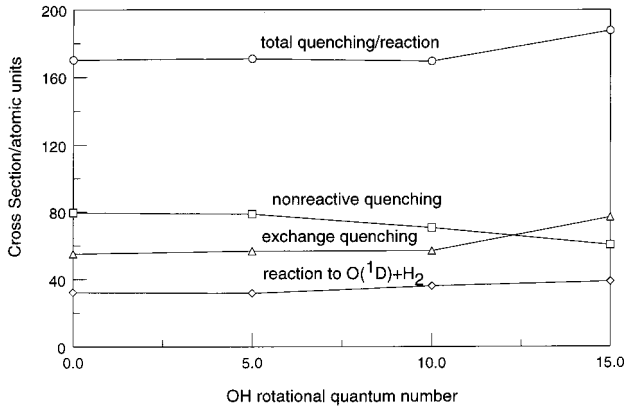

Figure 5. TSH cross sections for 2 kcal/mol translational energy as a function of the OH rotational quantum number *J*. Notation for curves is analogous to Figure 4a.

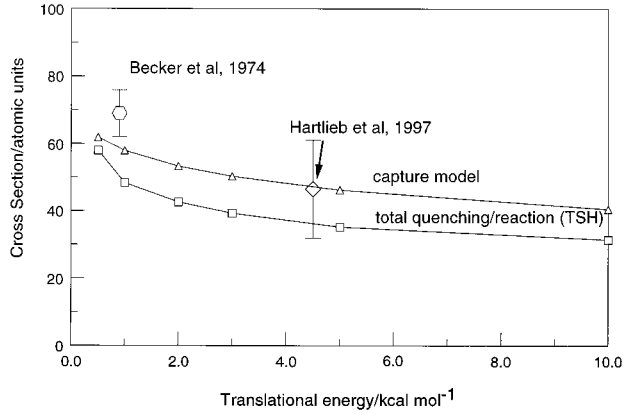

Figure 6. TSH cross section for total quenching plus reaction (squares), along with experimental estimates from refs 5 (diamond) and 6 (circle), and estimates from a diabatic capture model (triangles).

probability for reaction to give $O(^1D) + H_2$ is probably due to direct reaction that we occasionally see in trajectories, where the incoming H atom strikes the H atom in OH in an approximately collinear geometry, and directly abstracts it.

To study the influence of OH rotation, in Figure 5 we present cross section versus rotational quantum number *J* for total quenching reaction (T), nonreactive quenching (NQ), quenching with hydrogen exchange (QX), and reaction to $O(^1D) + H_2$(R). This figure shows that there is essentially no dependence on *J* for $J = 0-10$ and a weak dependence (increasing slightly) for high *J*. This behavior is exactly the opposite to the decrease with *J* that is observed or assumed in quenching of OH by rare gases and other nonreactive collision partners.[1,6] This reflects the fundamentally different mechanism for quenching for H + OH(A) which is dominated by complex formation rather than impulsive dynamics.

B. Thermally Averaged Cross Sections. To further study the behavior of σ_T, in Figure 6 we present TSH cross sections that have been averaged over a rotational Boltzmann distribution, and multiplied by the electronic statistical factor of 1/4. These results are for 300 K, but they are virtually indistinguishable from those at 1500 K. Also plotted in Figure 6 is the classical capture model result, and two experimental estimates of σ_T, one from the 300 K measurement of ref 5 and the other from the 1500 K estimate of ref 6.

The comparisons in Figure 6 show that the capture model cross section is consistently higher than TSH, with a similar energy dependence. Note that the capture model implicitly includes σ_X (exchange without quenching), but the TSH cross section σ_T does not. In addition, we will show later (section III.D) that there is a cross section comparable to σ_X associated with trajectories that form complexes but which are ultimately nonreactive. If these cross sections are subtracted from the capture model result (not shown), then the resulting "corrected" capture cross section is found to be in excellent agreement with TSH. However, this "fix" would not be available in a capture theory analysis without doing a TSH calculation, so what it really means is that capture theory will tend to overestimate quenching cross sections due to the presence of trajectories which are captured but which ultimately end up as H + OH-(A).

Figure 6 shows that the two experimental results are higher than TSH by 25−30%. This is reasonably good agreement, given the uncertainties in the experiments (±10% in the Becker et al. result and ±30% in the Hartlieb et al. result), but there are at least two sources of error in the theory that could also be involved. One is inaccuracy in the potential surface, and the other is contribution to the cross section from the triplet initial state. In studies of $O(^1D) + H_2$ it was found that thermal rate coefficients based on the DK surfaces agreed with experiment to within better than 10%,[8] so this provides one piece of data that would suggest that errors in the surface are not important. The role of triplet states is harder to judge, but a very recent study[15] has demonstrated that there can be substantial singlet−triplet coupling for OH(X) + H when the states are nearly degenerate, so this mechanism for the triplet states to contribute to quenching/reaction is at least a possibility.

C. Rate Coefficients for Quenching and Reaction. Table 2 presents the rate coefficients at 300 and 1500 K for the processes: total (T), nonreactive quenching (NQ), exchange quenching (XQ), reaction (R), and exchange without quenching (X). Included in the table are results for $J = 0$, 5, 10, and 15 and the rotational Boltzmann average. Also included in the table are previous estimates of the total quenching rate constant k_T. These estimates are derived from the same data as the cross sections in Figure 6, so the comparison with experiment is of the same quality (i.e., theory is 25−30% below experiment).

D. Product Energy Partitioning. Figure 7 shows how the average energy in product translation, rotation, and vibration depends on reagent translational energy for $J = 0$. Here we include results for (a) nonreactive quenching, (b) quenching with H atom exchange, and (c) reaction to $O(^1D) + H_2$. The results at 2 kcal/mol are also summarized in Table 1, along with the results of microcanonical statistical theory calculations. We see from Figure 7 that the average energy disposal varies with the specific process being considered, but the fractions of energy going into each degree of freedom are relatively invariant to reagent kinetic energy. The dependence on which process is considered depends in large measure on how much energy is available. The nonreactive quenching and hydrogen exchange processes both have an available energy of 88 kcal/mol or greater, and we see that translation and vibration are about equal, receiving 40−45% while rotation gets about 15%. Reaction to $O(^1D) + H_2$ has an exoergicity of 44 kcal/mol, but here translation gets most of the available energy.

Table 2 shows that this energy partitioning behavior is not consistent with a microcanonical distribution. This most likely arises because the intermediate complexes are too short-lived to be statistical. A simple calculation shows that the OH rotational angular momentum is not limited by the light atom released when nonreactive quenching or exchange quenching occur, so microcanonical theory with constrained angular momentum would not change the results significantly.

TABLE 2: Quenching/Reactive Rate Coefficients (in cm^3/s) as a Function of OH Rotational Quantum Number *J*, along with the Boltzmann Average, at 300 and 1500 K

	300 K					1500 K				
J	$k_T \times 10^{10}$	$k_{NQ} \times 10^{10}$	$k_{XQ} \times 10^{10}$	$k_R \times 10^{10}$	$k_X \times 10^{10}$	$k_T \times 10^{10}$	$k_{NQ} \times 10^{10}$	$k_{XQ} \times 10^{10}$	$k_R \times 10^{10}$	$k_X \times 10^{10}$
0	4.1	1.6	2.1	0.4	0.003	6.3	2.6	3.0	0.7	0.01
5	3.6	1.7	1.3	0.5	0.05	5.8	2.6	2.1	1.0	0.09
10	3.6	0.9	1.8	1.0	0.04	5.7	1.5	2.6	1.5	0.09
15	4.1	1.1	2.3	0.4	0.3	6.4	1.8	3.4	0.7	0.5
Boltzmann av	3.9	1.6	1.8	0.4	0.02	5.8	2.3	2.4	1.1	0.09
expt	5.0 ± 0.5[a]					8 ± 3[b]				

[a] Reference 5. [b] Reference 6.

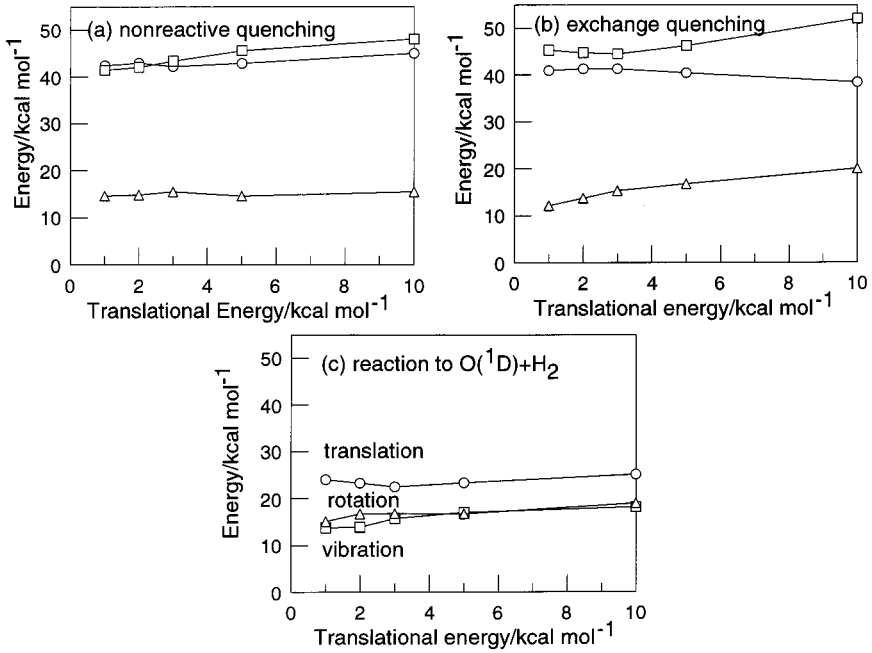

Figure 7. Average energy in product translation (circles), vibration (squares) and rotation (triangles) from the TSH calculations as a function of translational energy, for (a) nonreactive quenching, (b) quenching with H atom exchange, and (c) reaction to $O(^1D) + H_2$.

E. Rotational Energy Transfer. Here we consider cross sections for "pure" rotational energy transfer, denoted σ_{NR} earlier. These cross sections are often associated with the long-range part of the intermolecular potential, so to make sure that we have calculated these accurately, we performed several calculations using much larger impact parameters (up to 15 a_0) than in the studies presented so far. What we found was that impact parameters larger than 10 a_0 did not contribute to rotationally inelastic cross sections. In fact, almost all of the rotationally inelastic trajectories were part of the capture mechanism that normally produces electronic quenching or reaction. The total cross section for rotationally inelastic scattering (summed over J') is in fact about 60% of that for exchange without quenching, independent of E_T, except at energies below 1 kcal/mol where it becomes comparable with σ_X. This means that σ_{NR} is always less than 5 a_0^2, and the rate coefficient k_{NR} is approximately 0.02×10^{-10} cm^3/s at 300 K and 0.09×10^{-10} cm^3/s at 1500 K.

Rotationally inelastic scattering involves transitions from the initial rotational state to several possible rotational states J'. We find that the final state distribution is very broad, although not statistical. For example, at 2 kcal/mol, the cross sections starting from $J = 0$ are 0.5 a_0^2 for $J' = 1$, 0.4 a_0^2 for $J' = 2$, 0.3 a_0^2 for $J' = 3$, 0.3 a_0^2 for $J' = 4$, 0.1 a_0^2 for $J' = 5$, and 0.2 a_0^2 for $J' = 6$ with the sum over $J' \neq 0$ being 2.3 a_0^2. The observation of broad J' distributions is consistent with the complex formation as the dominant mechanism for nonreactive rotational energy transfer. Since σ_{NR} is much smaller than the quenching or reactive cross sections, it is clear that pure rotational energy transfer is too slow to compete with quenching or reaction.

IV. Conclusions

This paper has presented a quasiclassical trajectory surface hopping study of reaction and quenching of OH(A) in collisions with H atoms. The calculations were based on accurate ab initio potential surfaces, and it is encouraging to see that the overall cross sections and rate coefficients for quenching plus reaction are in good agreement with two previously derived values. What we have learned from this study is that this overall rate coefficient is determined by the long-range attractive part of the 2A′ potential surface rather than by the probability of nonadiabatic transitions to the 1A′ state (which is close to unity). We demonstrated that a capture model that assumes the most favorable orientation of the OH relative to the incoming H accurately describes the overall reaction cross sections, with the only errors arising from the few trajectories that return to OH(A) + H either via exchange or nonreactive scattering. The primary products of H + OH(A) collisions that surmount the centrifugal barrier are nonreactive quenching and quenching with hydrogen atom exchange. Reaction to give $O(^1D) + H_2$ accounts for about 25% of the products, with about equal probability for this occurring on the 1A′ and 2A′ potential surfaces. These cross sections are nearly independent of rotational quantum number, which is a very different result than is assumed in modeling

OH quenching by nonreactive partners (and which was previously used in modeling H + OH(A)[6]). We have also studied product energy partitioning for the several possible products of H + OH(A), and we find nonstatistical behavior that is consistent with a complex that undergoes very rapid decay. Finally, we have also determined cross sections for pure rotational energy transfer. These cross sections are also associated with the capture mechanism, and they are similar to those for exchange without quenching, corresponding to less than 5% of the total quenching/reaction cross sections.

Acknowledgment. This research was supported by NSF Grant CHE-9873892. We thank D. Markus and K. Kohse-Höinghaus for stimulating our interest in this problem.

References and Notes

(1) Kohse-Höinghaus, K. *Prog. Energy Combust. Sci*. **1994**, *20*, 203.
(2) Hogan, P.; Davis, D. D. *J. Chem. Phys*. **1975**, *62*, 4574. McDermid, I. S.; Laudenslager, J. B. *J. Chem. Phys*. **1982**, *76*, 1824. Copeland, R. A.; Crosley, D. R. *Chem. Phys. Lett*. **1984**, *107*, 295. Anderson, D. T.; Todd, M. W.; Lester, M. I. *J. Chem. Phys*. **1999**, *110*, 11117. Lester, M. I.; Loomis, R. A.; Schwartz, R. L.; Walch, S. P. *J. Phys. Chem. A* **1997**, *101*, 9195.
(3) Paul, P. H. *J. Quant. Spectrosc. Radiat. Transfer* **1994**, *51*, 511.
(4) Hartlieb, A. T.; Markus, D.; Kreutner, W.; Kohse-Höinghaus, K. *Appl. Phys*. **1997**, *B65*, 81.
(5) Becker, K. H.; Haaks, D.; Tatarczyk, T. *Chem. Phys. Lett*. **1974**, *25*, 564.
(6) Jeffries, J. B.; Kohse-Höinghaus, K.; Smith, G. P.; Copeland, R. A.; Crosley, D. R. Chem. *Phys. Lett*. **1988**, *152*, 160. Kienle, R.; Lee, M. P.; Kohse-Höinghaus, K. *Appl. Phys. B* **1996**, *62*, 583.
(7) Dobbyn, A. J.; Knowles, P. J. *Mol. Phys*. **1997**, *91*, 1107. Dobbyn, A. J.; Knowles, P. J. *Faraday Discuss*. **1998**, *110*, 247.
(8) Gray, S. K.; Petrongolo, C.; Drukker, K.; Schatz, G. C. *J. Phys. Chem*. **1999**, *103*, 9448.
(9) Gray, S. K.; Balint-Kurti, G. G.; Schatz, G. C.; Lin, J. J.; Liu, X.; Harich, S.; Yang, X. *J. Chem. Phys*. **2000**, *113*, 7330.
(10) Drukker, K.; Schatz, G. C. *J. Chem. Phys*. **1999**, *111*, 2451.
(11) Tully, J. C. *J. Chem. Phys*. **1990**, *93*, 161.
(12) Schatz, G. C.; Pederson, L. A.; Kuntz, P. J. *Faraday Discuss. Chem. Soc*. **1997**, *108*, 357.
(13) Gray, S. K.; Goldfield, E. M.; Schatz, G. C.; Balint-Kurti, G. G. *Phys. Chem. Chem. Phys*. **1999**, *1*, 1141.
(14) Kinsey, J. L. *J. Chem. Phys*. **1971**, *54*, 1206. Schatz, G. C.; Ross, J. *J. Chem. Phys*. **1977**, *66*, 2943.
(15) Hoffmann, M.; Schatz, G. C. *J. Chem. Phys*. **2000**, *113*, 9456.